Nanoparticles Modeling in Axially Injection Suspension Plasma Spray of Zirconia and Alumina Ceramics

Hong-Bing Xiong and Jian-Zhong Lin

(Submitted January 31, 2009; in revised form May 21, 2009)

Suspension plasma spray (SPS) is a thermal spray method in which nanoparticles are injected into the plasma jet with the help of suspension droplets to achieve thin and finely structured nanocoatings. The nanoparticles experience three in-flight stages: injection within the suspension droplets, discharge of the nanoparticle agglomerates after the evaporation of the suspension solvent, and tracking of the nanoparticle or agglomerates during the momentum and heat transfer with the plasma jet before coating. A numerical model is proposed in this paper for nanoparticle injection, discharge, acceleration, heating, melting, and evaporation. Initial values of suspension droplet size and agglomerate size are selected according to typical experimental data. Noncontinuum effects on particle acceleration and heating, known as Knudsen effects, are considered, as well as the influence of evaporation on the heat transfer. After a comparison with the experimental data, this nanoparticle model is applied for zirconia and alumina axially injected into the suspension plasma spray. Trajectory, velocity, and temperature of the in-flight nanoparticles are predicted for different initial sizes ranging from 30 nm to 1.5 μm; the distributions of the particle characteristics for multiple particles in the spray are also presented. The effects of powder size and material, power input, plasma gas flow rate, and standoff distance on the nanoparticle characteristics have been investigated and discussed.

1. Introduction

Suspension plasma spray (SPS) was developed as a new method of plasma spraying (Ref 1-6). In the SPS process, the feedstock of nanosize powder, mostly less than 5 μm in dimension, are dispersed in a liquid carrier and injected into the spray by the atomization device. The nanoparticles are small enough to form a suspension in the liquid carrier, and they are often aggregated in the solvent of the suspension. To make the coating, the suspension is first introduced into the plasma jet through an injection nozzle, typically a pneumatic atomizer that uses a pressurized gas to shear the liquid into a stream of droplets. The droplets evaporate under the plasma environment, and the carried nanoparticles are then discharged to the plasma jet. Using liquid suspension, much finer particles can be used to achieve thin and finely structured coatings, without common feeding problems encountered in the conventional direct powder injection. As a result, the final coatings are of improved characteristics compared with those applied by conventional thermal spraying in the aspect of having superior resistance to wear, erosion, and cracking.

Research studies have been conducted to understand the mechanism that governs the feedstock behavior in the suspension spray (Ref 1-6). It is reported that variations in the feedstock size and material may increase the difficulty in producing uniform microstructure of the coatings. Such variations especially the size distribution of in-flight nanoparticles and agglomerates, however, are common in the SPS process with a range from a few nanometers to tens of micrometers. Effects of size on the nanoparticle characteristics of in-flight velocity, temperature, and melting state are important to the controllability of coating structure and properties. The nanoparticles dynamic and thermal behavior under different operating conditions are very important in the application of suspension injection. Thus, it is necessary to develop a numerical model to describe the energy-transport process and predict the nanoparticle in-flight characteristics from the operating conditions of the spray.

Suspension plasma spray is a complicated process, which involves liquid feedstock preparation, atomization process, plasma jet generation, and interaction of plasma jet with the in-flight droplets and nanoparticles of broad size range. The initial diameter of the suspension droplets depends on the atomization methods, atomizer conditions, and properties of the liquid material. For pneumatic atomizer, the droplet size ranges from 5 to 100 μm, and initial droplet velocity ranges from 5 to 100 m/s (Ref 3). The agglomerate size and distribution in the liquid depend

Hong-Bing Xiong and Jian-Zhong Lin, Department of Mechanics, Zhejiang University, Hangzhou 310027, China; and Jian-Zhong Lin, China Jiliang University, Hangzhou 310018, China. Contact e-mail: hbxiong@zju.edu.cn.

Nomenclature	
C_p	specific heat, J/kg K
C_D	drag coefficient
D	diffusion coefficients, m^2/s
k	thermal conductivity, W/m K
L_m	latent heat of fusion, J/kg
L_v	latent heat of evaporation, J/kg
Nu	Nusselt number
Pr	Prandtl number, PR = $\eta C_p/k$
Q_{conv}	convection heat flux, W/m^3
Q_{rad}	radiation heat flux, W/m^3
Q_{vap}	vaporization heat flux, W/m^3
Sh	Sherwood number
r	radial coordinate, m
t	time, s
T_p	particle temperature, K
u	axial velocity, m/s
v	radial velocity, m/s
w	tangential velocity, m/s
V	plasma velocity vector, m/s
V_p	particle velocity vector, m/s
x	axial coordinate, m

Greek symbols	
α	weight fraction
η	viscosity, kg/s m
θ	azimuthal coordinate

Subscripts	
d	suspension droplet embedded with nanoparticles
g	plasma gas
p	solid nanoparticles or agglomerates
sl	solvent

on the solid powder size and properties, solvent material and concentration, and preparation method. Experiments show that the agglomerate sizes in different suspension are closely comparable regardless of initial particle size or solid concentration. For example, the agglomerate size ranges from 0.2 to 9 μm for zirconia and alumina nanoparticles in ethanol solvent (Ref 1). This study focuses on the in-flight process of the particles and select typical values of agglomerate size and atomized droplet size as input value of the simulation.

This paper proposes a numerical model for the in-flight behavior of nanoparticles in the suspension plasma spray, which includes the nanoparticle injection, suspension heating, particle discharge, tracking, heating, melting, and evaporation. Nanoparticle trajectory, velocity, and temperature in different in-flight stages were calculated with different particle material and initial size. The distributions of the particle characteristics for multiple particles in the spray are also presented. The priorities of operating conditions that influence the particle characteristics were investigated.

2. Mathematical Model

The suspension droplet or nanoparticle is treated as a discrete Lagrangian entity that exchanges mass, momentum, and energy with the plasma gas. The mathematical models for nanoparticles in suspension plasma spray system includes three submodels, namely, (1) heating of suspension droplet and discharge of the nanoparticles and agglomerates, (2) acceleration and tracking of individual particles, and (3) nanoparticles heating, melting, and evaporation.

Here, it is assumed that all the nanoparticle agglomerates have a uniform size of 5 μm for simplicity. A typical mean droplet size of 50 μm is assigned based on the commonly used pneumatic atomizer.

2.1 Heating of Suspension Droplets

Computational suspension droplets are generated at the points of injection and tracked throughout their flight. The droplet has the initial temperature of 300 K. Neglecting the thermal conduction and using the lumped thermal capacity model, the evolution of the droplet temperature can be expressed by:

$$T_d = T_{d,0} + \frac{Q_d}{m_d c_{p,d}} t \quad \text{if } T_d < T_{m,d}$$
$$T_d = T_{m,d} \quad \text{if } Q_d \leq m_d c_{p,d}\left(T_{m,d} - T_{d,0}\right) + m_d \alpha_{sl} L_{v,sl} \tag{Eq 1}$$

where $T_{d,0}$, Q_d, m_d, and $C_{p,d}$ are the initial droplet temperature, heat gain, mass, and the specific heat of the droplet, respectively. The specific heat of the droplet, $C_{p,d}$, is averaged based on the mass fraction of solid and solvent as $C_{p,d} = C_{p,p} (1 - \alpha_{sl}) + C_{p,sl}\alpha_{sl}$.

Assumed that the nanoparticle agglomerates are suspended randomly inside the droplet as shown in Fig. 1. When the solvent evaporates, the agglomerates at the droplet surface are discharged to the plasma jet. These agglomerates are generated in the simulation as new Lagrangian entities with the current parameters of position, droplet velocity, and temperature as the initial conditions.

2.2 Nanoparticles Acceleration and Tracking

Nanoparticle agglomerates then enter into the plasma jet and are subjected to acceleration and heating. They might explode into smaller pieces of aggregates or individual nanoparticles, as a result of the further evaporation of the solvent and the aerodynamic force of plasma gas acting on the aggregates. In this study, we examine the two extreme conditions of the aggregate explosion, namely, complete explosion to form individual nanoparticles with initial size or no explosion to keep the aggregate as is and melt as a large particle. Once the remaining solvent is totally vaporized, it is assumed that the explosion occurs for the case of complete explosion; for the case of no explosion, the aggregate continues flying in the plasma jet. Currently, the transport properties of the aggregates are averaged based on the solid and solvent mass fraction, though it might be different from that of the bulk material because of the thermal resistance between the particle boundaries.
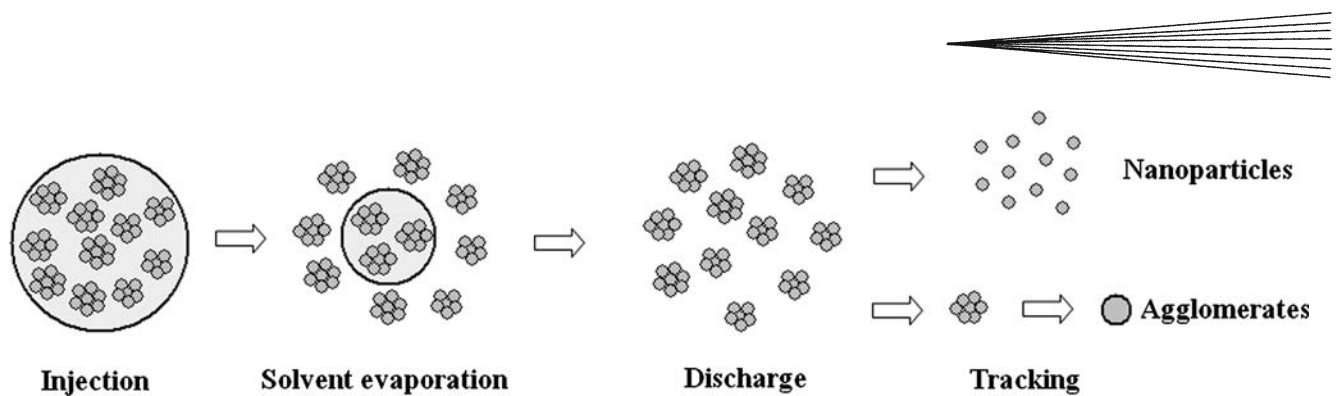
Fig. 1 Nanoparticle injection, discharge, and tracking

To track the nanoparticles or nanoparticle agglomerates, the drag force is assumed to be the only prominent driving force for the small particle size less than 100 μm (Ref 7). Assuming the spherical shapes of the nanoparticles and agglomerates, the momentum transfer between the particle and the plasma can be described by

$$\vec{F}_p = m_p \frac{d\vec{V}_p}{dt} = \pi r_p^2 C_D \frac{\rho |\vec{V} - \vec{V}_p|(\vec{V} - \vec{V}_p)}{2} \tag{Eq 2}$$

where V is the gas velocity including the turbulent fluctuation, C_D is the drag coefficient expressed by

$$C_D = \left(\frac{24}{\mathrm{Re}_p} + \frac{6}{1 + \sqrt{\mathrm{Re}_p}} + 0.4 \right) f_{prop}^{-0.45} f_{Kn}^{0.45} \tag{Eq 3}$$

where the particle Reynolds number, Re_p, is defined as $2\rho_f r_p |\vec{V} - \vec{V}_p|/\mu_f$; f_{prop} and f_{Kn} represent the effects of variable plasma properties and noncontinuum, respectively; the formulas for f_{prop} can be found in Ref 7; f_{Kn} is expressed by

$$f_{Kn} = \left[1 + \left(\frac{2-a}{a} \right) \left(\frac{\gamma_w}{1 + \gamma_w} \right) \frac{4}{\mathrm{Pr}_w} \mathrm{Kn} \right] \tag{Eq 4}$$

where Kn is the Knudsen number based on the effective mean free path. Note that the momentum transfer between the suspension droplets and the plasma jet is calculated as the same method as that of the nanoparticles. In addition, Knudsen number accounts for the size effect, that is, f_{Kn} has values of 0.005 to 0.1 for nanoparticles and 0.994 to 0.996 for suspension droplets.

Equation 2 is then used to calculate the particle velocity and trajectory. Then the local conditions of the plasma gas around the particles can be determined including the gas temperature and heat-transfer coefficient, which is used to calculate the particles heating and melting.

2.3 Nanoparticles Heating, Melting, and Evaporation

A one-dimensional model is used for nanoparticle heating and melting, in which the spherical shape of the particle is assumed as in Fig. 2. The agglomerates are also treated in one-dimensional spherical coordinate, without considering the nanoparticle distribution before melting. The internal convection within the molten part of the
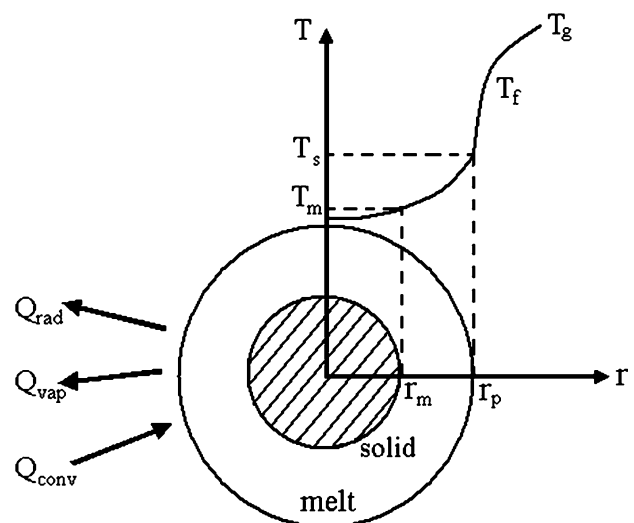

Fig. 2 Particle heat transfer

particle is neglected. The temperature distribution inside the particle is described by conduction:

$$\rho_p C_p \frac{\partial T_p}{\partial r} = \frac{1}{r^2} \frac{\partial}{\partial r} \left(k_p r^2 \frac{\partial T_p}{\partial r} \right) \tag{Eq 5}$$

with zero temperature gradient in the particle center, and the particle surface is energy balanced as:

$$\left. \frac{\partial T_p}{\partial r} \right|_{r=0} = 0 \text{ and } 4\pi r_p^2 \left(k_p \frac{\partial T_p}{\partial r} \right) \bigg|_{r=r_p} = \dot{Q}_{conv} - \dot{Q}_{vap} - \dot{Q}_{rad} \tag{Eq 6}$$

where the convection, radiation, and evaporation latent heat fluxes $\dot{Q}_{conv}, \dot{Q}_{vap}$, and $\dot{Q}_{rad}$ are expressed as $4\pi r_p^2 h_f(T_f - T_s)$, $\dot{m}_v L_v$, and $4\pi r_p^2 \varepsilon_p \sigma_s \left(T_s^4 - T_\infty^4 \right)$, respectively. The film temperature, T_f, defined by $(T_s + T_g)/2$ as shown in Fig. 2, is introduced to deal with the steep temperature gradient in the boundary layer around the particle. Only the radiation between the particle surface and the environment is considered in the case of optically thin plasma gas. The heat-transfer coefficient, h_f, can be calculated from:

$$Nu = \frac{2h_f r_p}{k_f} = \left(2.0 + 0.6\mathrm{Re}^{1/2}\mathrm{Pr}^{1/3} \right) f_{prop} f_{Kn} f_v \tag{Eq 7}$$

where f_v accounts for the effect of mass transfer due to evaporation:

$$f_v = \frac{\dot{m}_v c_{p,f}/2\pi r_p k_f}{\exp\{\dot{m}_v c_{p,f}/2\pi r_p k_f\} - 1} \qquad \text{(Eq 8)}$$

f_v approaches one when the evaporation mass rate $\dot{m}_v$ is close to zero. f_v is smaller than one when $\dot{m}_v$ is larger than zero. This indicates that the convective heat flux becomes smaller when accounting for the evaporation. An additional constraint of energy balance at the melting interface r_m is also considered:

$$\left(k_p \frac{\partial T_p}{\partial r}\right)\Bigg|_{r=r_m^-} - \left(k_p \frac{\partial T_p}{\partial r}\right)\Bigg|_{r=r_m^+} = L_m \rho_p \frac{dr_m}{dt} \qquad \text{(Eq 9)}$$

The evaporation mass rate, $\dot{m}_v$ is controlled either by the vapor diffusion or the heat transfer through the boundary layer around the particle. When the particles are heated to the melting point in the plasma gas, the vapor diffusion rate through the boundary layer is low and the heat gain of the particle is large enough to meet the latent heat of vaporization. However, when the particle surface temperature approaches the boiling point, the vapor diffusion rate could be so high that the energy needed to overcome the latent heat of vaporization is balanced by the net heat transfer to the particle. Therefore, the evaporation rate is limited by the minimum of the vapor diffusion rate and the net heat gain of the particle:

$$\dot{m}_v = \min\left\{2(\bar{\rho}D_g)_f \pi r_p \ln(1+B)\text{Sh}, \quad \dot{Q}_{net}/L_v\right\} \qquad \text{(Eq 10)}$$

where D_g is the mass-transfer coefficient, Sh is the Sherwood number representing convective mass transfer, and B is the mass-transfer number, which is related to the local mass fraction of vapor in the gas phase and the vapor concentration on the droplet surface.

2.4 Determination of the Plasma Jet Conditions

The plasma jet provides the energy source to speed and heat the particles. A well-established numerical code of plasma spray, called LAVA-P-3D (Ref 8), is used to determine the conditions of the direct current plasma jet. This code calculates the Navier-Stokes equations of the plasma jet as a compressible, continuous multicomponent, chemically reacting ideal gas with temperature-dependent thermodynamic and transport properties. Turbulent fluctuation of plasma jet is calculated by the k-ε model. The effect of in-flight particles on the plasma is neglected for this dilute spray system.

3. Numerical Setup

The present study is conducted for a direct-current suspension plasma spray system that uses Mettech Axial III spray gun (Northwest Mettech, North Vancouver, Canada). Table 1 lists the basic operating conditions, which are set the same as the experimental data in Ref 1. Six cases with different operating conditions, as shown in Table 2,

Table 1 Baseline operating conditions of single particle injection

Processing parameters	Values	
Plasma gas conditions		
Total plasma gas flow rate, slm	245	
Gas composition: Ar, N₂, H₂	75%, 10%, 15%	
Power input, kW	85	
Power efficiency	0.7	

Feedstock conditions	ZrO₂	Al₂O₃
Solid content in suspension	10%	10%
Initial nanoparticle size, nm	30, 40, 50, 60	43, 1500
Initial suspension droplet size, μm	50	50
Initial agglomerate size, μm	5	5
Standoff distance, cm	5	5

slm, standard liter per minute, 1 slm = 16.67 cm³/s

Table 2 Varied operating conditions of multiple particles injection

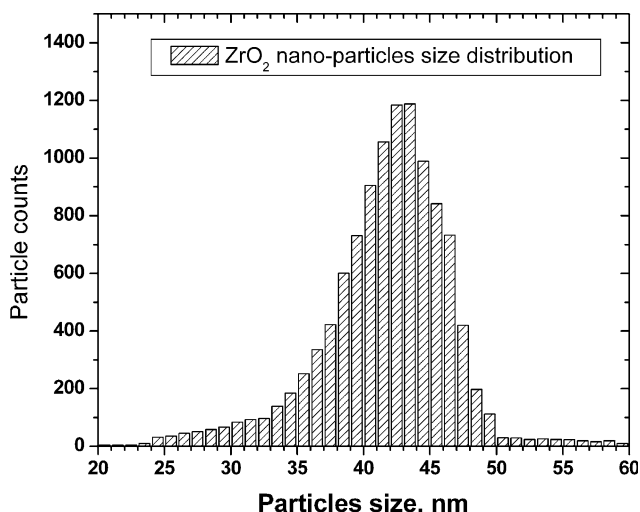| Case No.	ZrO₂ particle diameter, nm	Al₂O₃ particle diameter, nm	Mass fraction of ZrO₂/Al₂O₃	Power input, kW	Gas flow, slm
1	20-60	43	40/60	85	245
2	20-60	1500	40/60	85	245
3	20-60	43	40/60	110	245
4	20-60	1500	40/60	110	245
5	20-60	43	40/60	110	275
6	20-60	1500	40/60	110	275

Table 3 Particle properties

Property	Material ZrO₂	Al₂O₃
Solid density, kg/m³	5.89×10^3	3.9×10^3
Liquid density, kg/m³	5.89×10^3	3.9×10^3
Solid thermal conductivity, W/m K	2.0	4.3
Liquid thermal conductivity, W/m K	3.0	4.3
Solid specific heat, J/kg K	580	448
Liquid specific heat, J/kg K	713	448
Melting temperature, K	2950	2323
Boiling temperature, K	5000	3253
Latent heat of melting, J/kg	8×10^5	3×10^5
Latent heat of vaporization, J/kg	6×10^6	7×10^6

Table 4 Solvent properties

Material	Ethanol
Density, kg/m³	0.8×10^3
Specific heat, J/kg K	2400
Latent heat of vaporization, J/kg	9.25×10^5
Boiling temperature, K	351

are investigated to examine the effects of powder size, power supply, and gas flow rate on the particles characteristics. The nano- or microsize powder of ZrO₂ and Al₂O₃ using the suspension of ethanol are injected, with their material properties summarized in Table 3 and 4,

Fig. 3 Particle diameter distributions for the case of nonuniform size

(a)

(b)

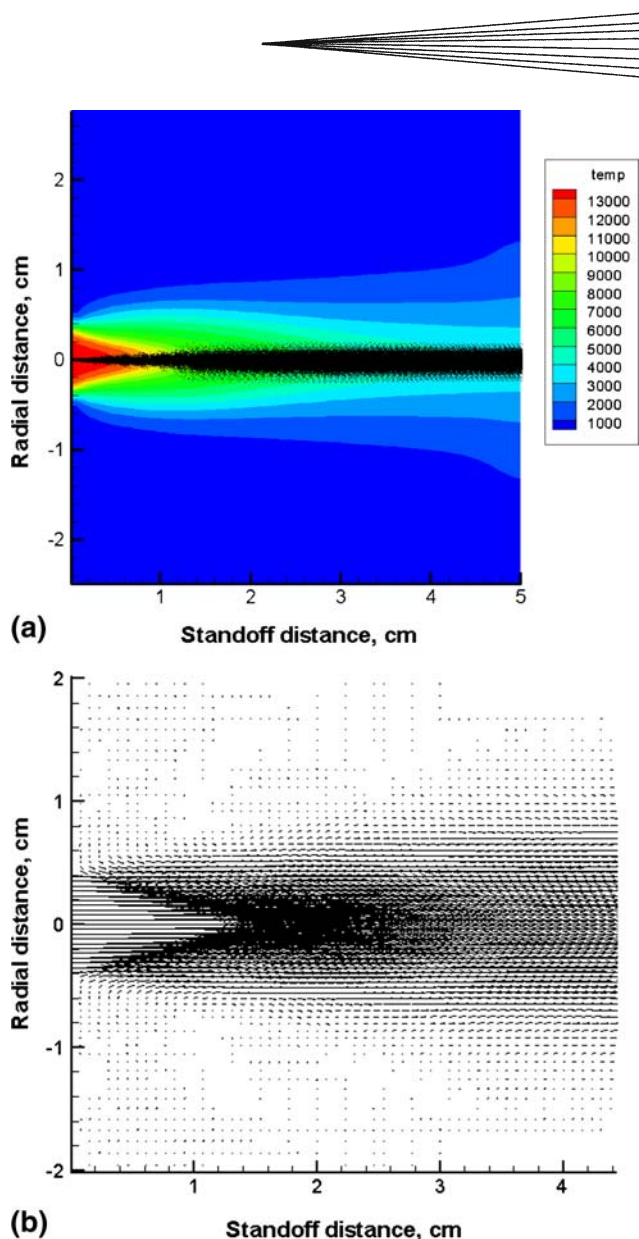**Fig. 4** (a) Gas temperature and particle position. (b) Gas velocity in suspension plasma spray

respectively. The ZrO_2 particle size used in this study has the range of 20 to 60 nm, as shown in Fig. 3. The Al_2O_3 particles have size of 43 nm in cases 1, 3, and 5, while in cases 2, 4, and 6, the Al_2O_3 particles have size of 1.5 μm.

At the nozzle exit, the temperature and axial velocity of the plasma jet are estimated from the empirical expressions (Ref 9) of $v(r) = V_{cl}[1 - (r/R_i)^{1.2}]$, and $T(r) = (T_{cl} - T_w)[1 - (r/R_i)^6] + T_w$, where V_{cl} and T_{cl} are the maximum values of plasma velocity and temperature matched with the known flow rate and the power supply, whereas T_w is the wall temperature. Zero velocity and ambient temperature of 300 K are set at the atomizer wall. The downstream of the plasma jet is taken as the open-boundary condition, without considering the substrate.

The simulation of the plasma jet is based on a two-dimensional cylindrical domain with mesh size of 57×66 in the radial and axial lengths of 6 and 5 cm, respectively. The suspension droplet and the nanoparticles are generated and tracked in the three-dimensional Cartesian coordinate, provided the symmetrical plasma jet condition as shown in Fig. 4. Mesh size of 50 in one-dimensional spherical domain is used inside each particle to simulate the heating and melting behavior. The suspension droplets are assumed to have an initial temperature of 300 K, a velocity of 50 m/s, and a diameter of 50 μm. About 10,000 nanoparticles are injected in the flow within the suspension droplets.

4. Validation of Numerical Model

The LAVA-P-3D code used in this study has been validated through the original well-tested LAVA 2D code; both the plasma jet and the microparticle injection have been proved to work correctly (Ref 7-9). In order to further validate this code for the nanoparticle behavior, the numerical results have also been compared with experimental data; in this case, the nanoparticle average velocity and temperature is compared with the published

experiment data in Ref 1. Their experiment used the Mettech Axial III spray system, with spray conditions as cases 1 and 2 listed in Table 1. The experimental particle velocity and temperature were measured by the diagnostic system Accura-Spray G2 (Tecnar Automation, St. Bruno, Canada) based on particle ensemble signals rather than the signal from individual particles. The measurements are taken at the standoff distance of 50 mm.

The simulated particle temperature and velocity are calculated by recording each particle temperature and velocity arriving at the substrate location and averaging them based on the mass fraction. The predicted particle characteristics of averaged T_p and V_p are plotted against the experimental data in Fig. 5 for cases 1 and 2. A good agreement between the simulation results and experimental data has been obtained; the difference between the experiment and simulation is within 10%.
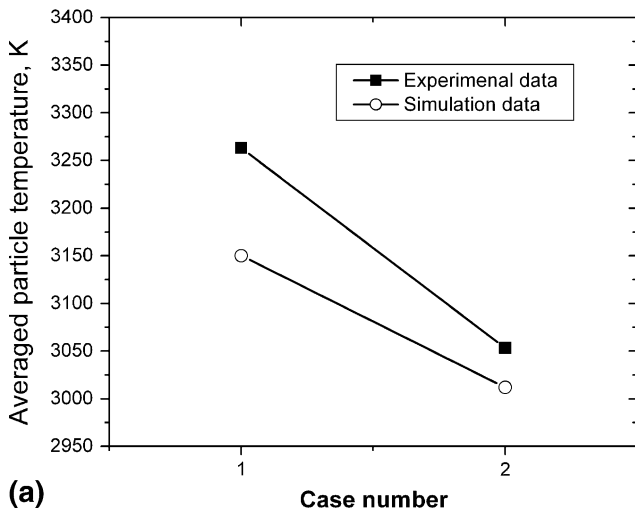
(a)
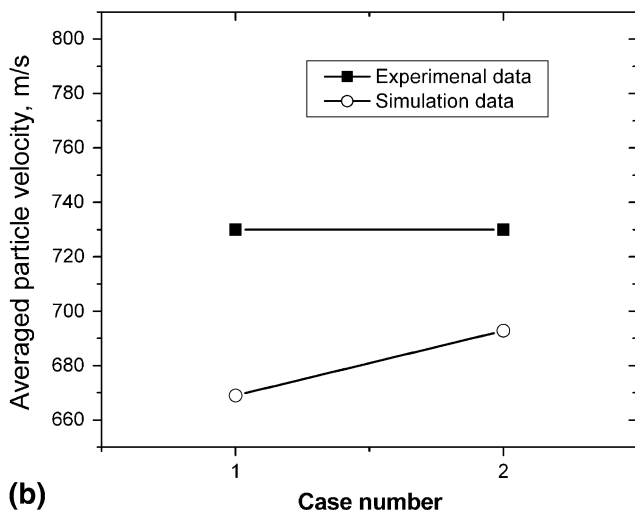
(b)

Fig. 5 Simulation results of averaged particle temperature and velocity at standoff distance 50 mm for cases 1 and 2 and comparison with the published experimental data (Ref 1)

5. Results and Discussion

Nanoparticle and agglomerate behavior has been studied in the suspension plasma spray process. The single particle injection is firstly investigated using the baseline operating conditions of Table 1. Two types of feedstock ZrO_2 and Al_2O_3 are investigated. The Al_2O_3 particle size is 43 nm and 1.5 μm, ZrO_2 particle size is 30, 40, 50, and 60 nm, and both of them have an agglomerate size of 5 μm. Such nanoparticle size range is typically used in experiments, for example, in Ref 1. Besides the single particle injection, the multiple particle behavior of mixture feedstock in the same suspension and under different plasma conditions, as listed in Table 2, are investigated. For single particle injection, the velocity intensity is the mean value of 50 m/s, and the velocity direction is 0° with regard to the axis. For the multiple particle injection, the initial velocity has certain deviation from the mean value
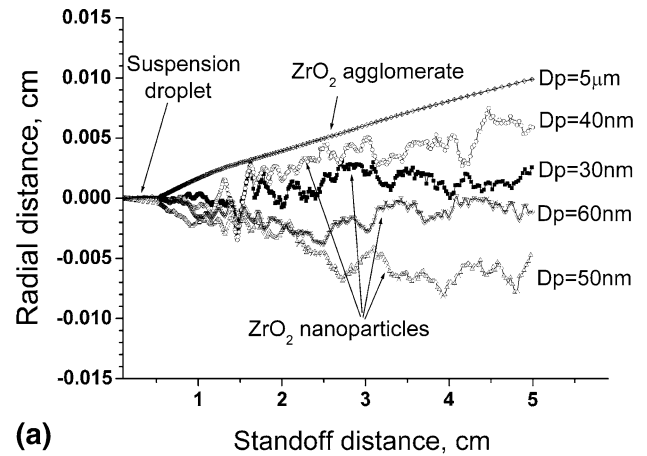

(a)
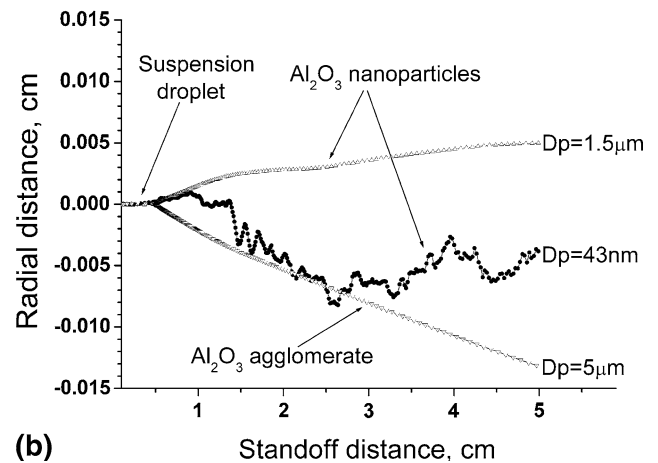
(b)

Fig. 6 Trajectories of zirconia and alumina nanoparticles of different sizes

of intensity and the zero direction. Here, 5% random deviation of velocity intensity and 20° deviation of the velocity direction are used for multiple particles cases. Results of single particles are shown in Fig. 6 to 8 and results of multiple particles in Fig. 9 and 10.

5.1 Results of Plasma Jet and Nanoparticles Tracking

The gas temperature contour and velocity vector of the baseline case are shown in Fig. 4(a) and (b), respectively. In Fig. 4(a), each dot represents a computational droplet or nanoparticle. The core of the plasma jet, at the distance of 1 cm from the torch exit, has very high temperature and velocity, more than 10,000 K and 2000 m/s. The droplet suspension resides in the plasma core and rapidly heats up to evaporation. After the discharge of agglomerate and nanoparticles, particles flying through the plasma jet are driven to a high speed up to 2500 m/s, and heated up to 4500 K.

The in-flight position, velocity, and temperature of the particles are highly related with particle trajectory,
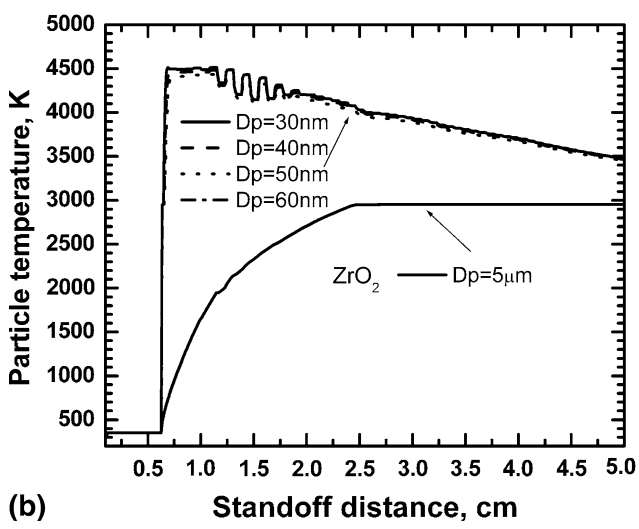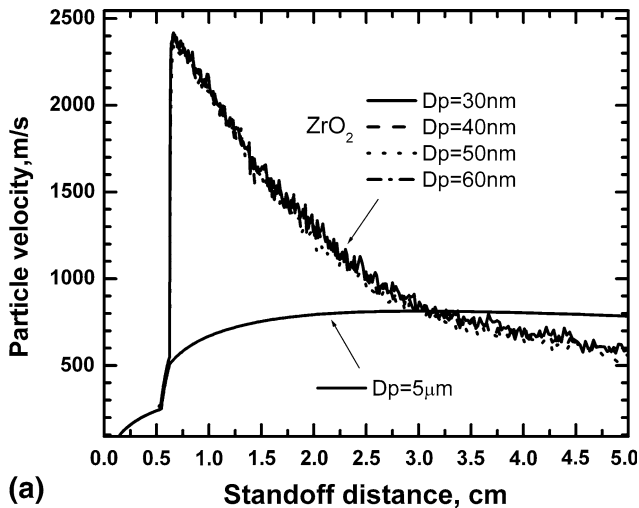
Fig. 7 Effects of particle size on (a) single zirconia nanoparticle velocity and (b) temperature
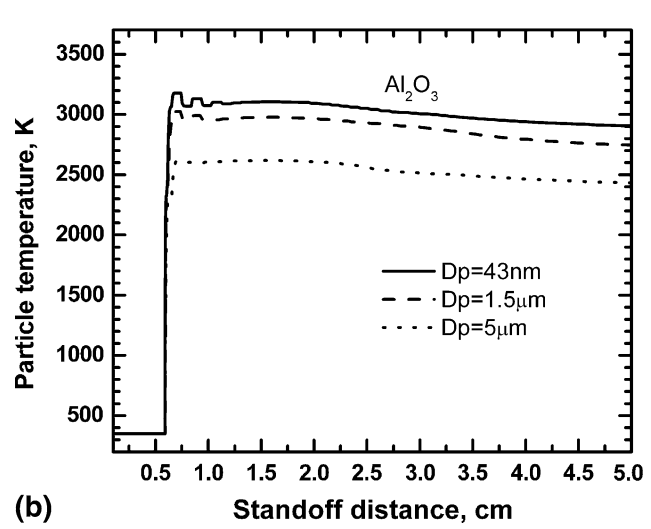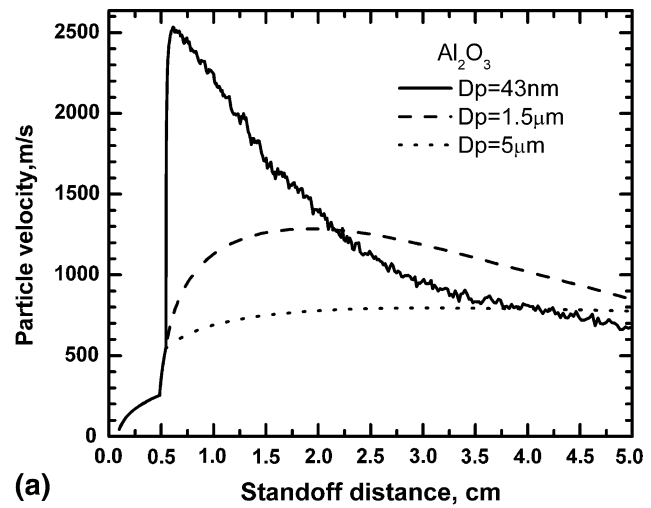
Fig. 8 Effects of particle size on (a) single alumina nanoparticle velocity and (b) temperature

surrounding gas condition, particle size, and properties. Figure 6 shows nanoparticle or agglomerate trajectory of ZrO_2 and Al_2O_3, respectively. Each particle is injected in the torch axis. Results show that the radial displacement is quite small, about 0.01 cm. Nanoparticles have different trajectories compared to the microsize agglomerates. The microsize suspension droplet is accelerated steadily by the gas stream, and its trajectory goes straight. When the suspension solvent vaporized at the standoff distance of about 0.5 to 0.7 cm, the nanoparticle or the agglomerates are discharged to the plasma jet. For the nanoparticles, the trajectories are highly fluctuating since the inertia is small and thus more sensitive to the gas turbulence. It should be pointed out that the turbulence model is important for the calculation of the nanoparticles tracking. Though k-ε model could provide quantitative results of the gas turbulent energy, a better turbulence model such as large eddy simulation (Ref 10, 11) would be helpful for more a accurate prediction of the nanoparticles trajectories.
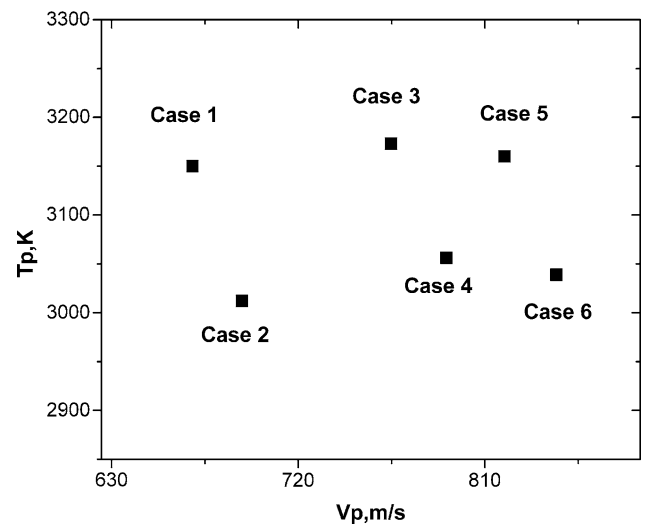
Fig. 9 Simulated averaged particle velocity and temperature at standoff distance 50 mm of cases 1 to 6
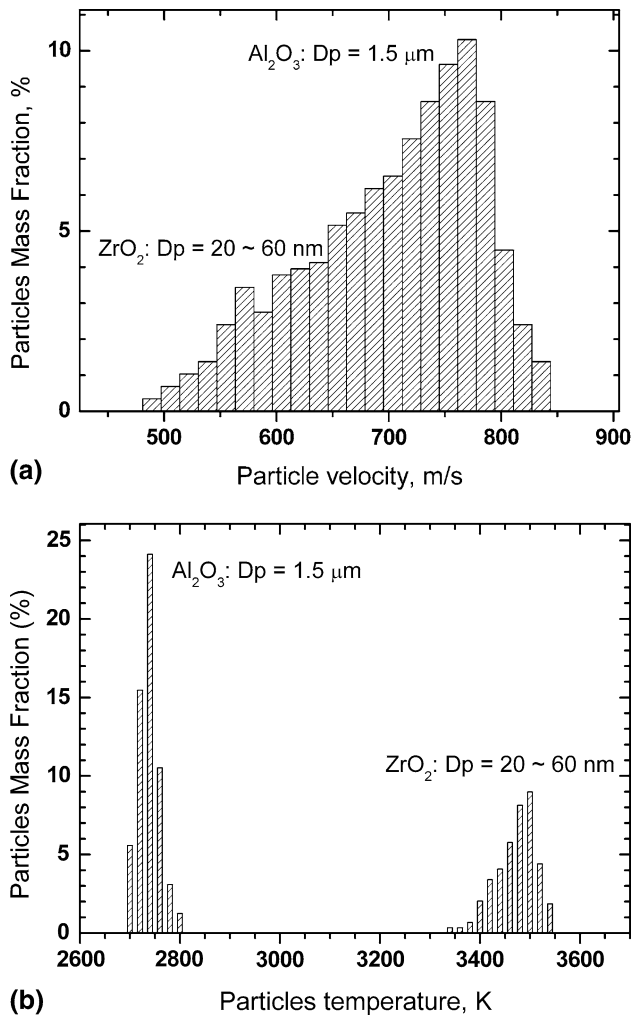
Fig. 10 Statistical distributions of (a) multiple particle velocity and (b) temperature in case 2

5.2 Nanoparticles Velocity and Temperature

Figures 7 and 8 depict the nanoparticle velocity and temperature during in-flight for ZrO_2 and Al_2O_3, respectively. All the nanoparticles undergo two stages of flight—flying within the microsize suspension droplet and flying of nanosize particles or agglomerates. During the first stage, droplet is accelerated and rapidly heated to the boiling point of the solvent. When the suspension droplet is continually evaporated, the nanoparticle agglomerates originally embedded in the evaporated solvent are then discharged to the plasma jet. In current case, the agglomerates are discharged to the plasma jet at the standoff distance of 0.5 to 0.7 cm, depending on the particle material properties. Zirconia nanoparticles are discharged later because of its higher specific heat compared to alumina. Here, the suspension droplet has constant size and each single particle is located at the droplet center. If considering the droplet size distribution from atomization process as in nature, the discharge location will be different for different nanoparticles.

After being discharged to the plasma jet, the nanoparticles begin the second stage of flight. It is possible that the nanoparticles stay within the agglomerate or explode to free nanoparticle. For the free nanoparticle, the speeding rate is increased immediately after the discharge. When the nanoparticles are further discharged to the plasma jet after agglomerate explosion, its velocity and temperature are steeply increased, followed by a slow deceleration and cooling rate downstream of the spray. The main reason for this phenomenon is that the mass of the nanoparticle is much smaller than that of their parent agglomerate and suspension droplet. For the nanoparticle agglomerates, the speeding and heating rate are smaller compared to the nanoparticles. However, the agglomerates have higher impact velocity than the nanoparticles because of their lower deceleration rate downstream of the spray, whereas its impact temperature is lower. For ZrO_2 agglomerate, the surface temperature is at the melting point upon impact, but the interior of the agglomerate is not totally melted due to its large latent heat of melting and high melting temperature.

The particle size and material affect particle acceleration and heating. As shown in Fig. 7, the ZrO_2 nanoparticles with size of 30 to 60 nm have similar impact velocity of mean value of 578 m/s with standard deviation of 22 m/s and similar impact temperature of 3464 K with standard deviation of 40 K. One reason is that the single nanoparticles travel close to the axis and experience the same gas environment; the other reason is their small thermal resistance and small inertia, which results in small values of $T_g - T_p$ and $V_g - V_p$. Thus, the ZrO_2 particles with nanosize range have similar T_p and V_p during in-flight, with small deviation resulting from the fluctuating trajectories.

For Al_2O_3 in Fig. 8, the nanoparticle with large size of 1.5 μm has a lower temperature and a higher velocity than the nanosize particle of 43 nm, since the large particle has higher thermal capacity to be overcome and larger inertia to be decelerated. Note that the velocity of the Al_2O_3 particle with size 1.5 μm of is even higher than that of the agglomerates within the standoff distance of 50 mm; while its velocity would be lower than that of the agglomerate beyond this distance due to the rapid deceleration by the gas. Compared to ZrO_2, the Al_2O_3 particles have the same range of velocity but different temperature (see Fig. 7 and 8). Because the boiling temperature of the alumina is 1747 K lower than that of zirconia, which limits the upper temperature that the Al_2O_3 particles could reach.

5.3 Effects of Operating Conditions on Multiple Particle Characteristics

Cases 1 to 6 with varied operating conditions as listed in Table 2 are investigated. Other operating conditions are the same as in Table 1. Figure 9 shows the particle characteristics, that is, average particle velocity and temperature, of these cases. Compared to cases 1 and 2, results of cases 3 and 4 show that the average V_p increases obviously and T_p increases slightly with increasing power input.
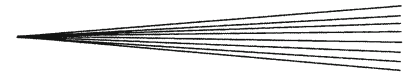
High power input makes both the gas temperature and velocity higher, and thus more momentum and heat is transferred to the particle. However, the heat transfer is limited by the heat resistance of plasma jet, for example, the low thermal conductivity of primary plasma gas of Ar. Results of cases 5 and 6 show the average V_p and T_p with continued increase in plasma gas flow rate along with an increase of power input. Again, V_p increases significantly. T_p increases compared to cases 1 and 2, but decreases compared to cases 3 and 4. The reason is that for same power input, a high gas flow rate increases the gas velocity but decreases the gas temperature.

For the combination of small nanoscale and large microscale particles as in cases 2, 4, and 6, the statistical distributions of the particle velocity and temperature are important to study. Figures 10(a) and (b) show the distributions of multiple particle velocity and temperature, respectively, with ZrO_2 of 20 to 60 nm and Al_2O_3 of 1.5 μm in case 2. Obviously, there are two peaks in the particle temperature distribution: one peak of 3500 K is caused by the small ZrO_2 nanoparticles, and the other peak of 2740 K is caused by the large Al_2O_3 nanoparticles. The two peaks of the particle velocity distribution, which is one peak of 570 m/s caused by the small ZrO_2 nanoparticles and the other peak of 770 m/s caused by the large Al_2O_3 nanoparticles, are not visible since the mean values of particle velocity are close and the deviation is large.

6. Conclusions

A numerical particle model is proposed to study nanoparticle tracking, acceleration, heating, melting, and evaporation in suspension plasma spray. The nanoparticles embedded in the suspension droplet are injected into the plasma jet. The droplet evaporation, discharge of the nanoparticles and agglomerates, in-flight behavior of the nanoparticles are calculated, considering the noncontinuum effects and the influence of the evaporation on the heat transfer. After validation with the experimental data, this heating and acceleration model for nanoparticles is applied to simulate the suspension plasma spray process with axially injected nanoparticles of zirconia and alumina suspended in the solvent of ethanol. This study investigated the effects of nanoparticle size, particle material, and plasma operating conditions on the particle characteristics. The results show that the trajectory of the suspension droplet and agglomerates follows steadily in the injection direction with certain expansion angle, while the nanoparticles have fluctuating trajectories. Powder size has a major effect on the particle temperature and a minor effect on the particle velocity. Nanoparticles have similar temperature and velocity if they experience the same gas environment. Large nanoparticles have lower temperature and may have a higher velocity depending on the local gas velocity. The average V_p increases obviously, but T_p increases slightly with increasing power input, and increasing gas flow rate increases the average V_p monotonously, and average T_p may increase or decrease depending on the gas temperature.

References

1. F. Tarasi, M. Medraj, A. Dolatabadi, J. Oberste-Berghaus, and C. Moreau, Effective Parameters in Axial Injection Suspension Plasma Spray Process of Alumina-Zirconia Ceramics, *J. Therm. Spray Technol.*, 2008, **17**(5-6), p 685-691
2. O. Tingaud, A. Grimaud, A. Denoirjean, G. Montavon, V. Rat, J.F. Coudert, P. Fauchais, and T. Chartier, Suspension Plasma-Sprayed Alumina Coating Structures: Operating Parameters Versus Coating Architecture, *J. Therm. Spray Technol.*, 2008, **17**(5-6), p 662-670
3. C. Marchand, C. Chazelas, G. Mariaux, and A. Vardelle, Liquid Precursor Plasma Spraying: Modeling the Interactions Between the Transient Plasma Jet and the Droplets, *J. Therm. Spray Technol.*, 2007, **16**, p 5-6
4. J. Fazilleau, C. Delbos, V. Rat, J.F. Coudert, P. Fauchais, and B. Pateyron, Phenomena Involved in Suspension Plasma Spraying Part 1 Suspension Injection and Behavior, *Plasma Chem. Plasma Process.*, 2006, **26**, p 371-391
5. J. Oberste Berghaus, J.G. Legoux, C. Moreau, F. Tarasi, and T. Chraska, Mechanical and Thermal Transport Properties of Suspension Thermal Sprayed Alumina-Zirconia Composite Coatings, *J. Therm. Spray Technol.*, 2008, **17**(1), p 91-104
6. P. Fauchais, R. Etchart-Salas, V. Rat, J.F. Coudert, N. Caron, and K. Wittmann-Teneze, Parameters Controlling Liquid Plasma Spraying: Solutions, Sols, or Suspensions, *J. Therm. Spray Technol.*, 2008, **17**(1), p 31-59
7. Y.P. Wan, V. Prasad, G.-X. Wang, S. Sampath, and J.R. Fincke, Model and Powder Particle Heating, Melting, Resolidification, and Evaporation in Plasma Spraying Processes, *J. Heat Transfer*, 1999, **121**, p 691-699
8. H.B. Xiong, L.L. Zheng, S. Sampath, R.L. Williamson, and J.R. Fincke, Three-Dimensional Simulation of Plasma Spray: Effects of Carrier Gas Flow and Particle Injection on Plasma Jet and Entrained Particle Behavior, *Int. J. Heat Mass Transfer*, 2004, **47**, p 5189-5200
9. J.D. Ramshaw and C.H. Chang, Computational Fluid Dynamics Modeling of Multi-component Thermal Plasmas, *Plasma Chem. Plasma Process.*, 1992, **12**, p 299-325
10. G. Mariaux and A. Vardelle, 3-D Time-Dependent Modelling of the Plasma Spray Process. Part 1: Flow Modelling, *Int. J. Therm. Sci.*, 2005, **44**, p 357-366
11. E. Meillot, D. Guenadou, and C. Bourgeois, Three-Dimension and Transient D.C. Plasma Flow Modeling, *Plasma Chem. Plasma Process.*, 2008, **28**(1), p 69-84